

Supporting Information

Mono-*N*-Protected Amino Acid Ligands Stabilize Remarkable Dimeric Palladium(II) Complexes of Importance to C-H Functionalization

Joseph J. Gair,¹ Brandon E. Haines,² Alexander S. Filatov,¹ Djamaladdin G. Musaev,^{2*} and Jared C. Lewis^{1*}

¹Department of Chemistry, The University of Chicago, Chicago Illinois, 60637, United States

²Cherry L. Emerson Center for Scientific Computation, Emory University, 1515 Dickey Drive, Atlanta Georgia 30322, United States

E-mail: jaredlewis@uchicago.edu , dmusaev@emory.edu

Table of Contents

S2.1. Computational Methodology	S2
S2.2. Comparison of Experimental and Computational Dimer Structures	S3
S2.3. Dimerization Energies and Conformations of Dimeric Structures	S4
S2.4. Substrate Effect	S5
S2.5. C-H Activation with MPAA Dimer and Monomer	S6
S2.6. Computational Analysis of Pd-C Bond Iodination in Cyclopalladated MPAA Dimer and Monomer Complexes	S8
S2.7. Energies for Calculated Structures	S10
S2.8. References	S12

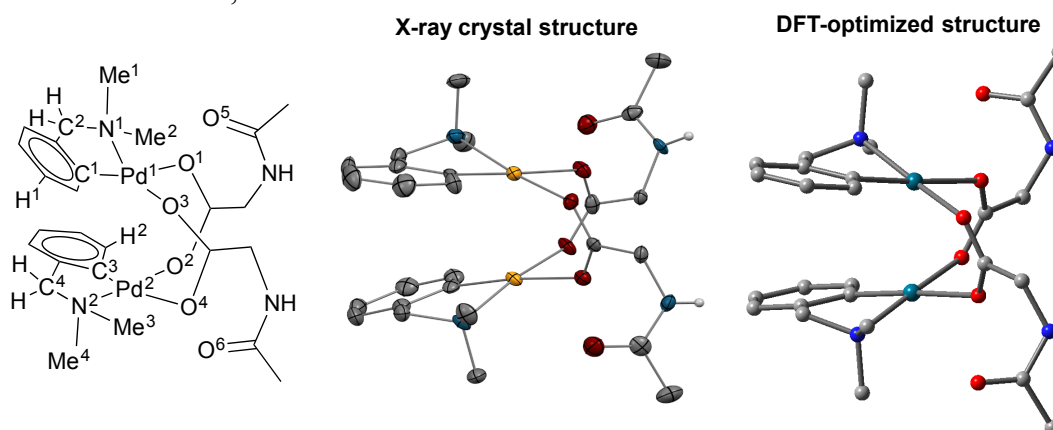
S2.1. Computational Methodology

The Gaussian 09 suite of programs¹ was used for all described calculations. Geometry optimizations and frequency calculations for all reported structures were performed at the B3LYP-D3BJ/[6-31G(d,p) + Lanl2dz (Pd, I)] level of theory (B3LYP-D3BJ/BS1) with the corresponding Hay-Wadt effective core potential for Pd and I and Grimme's empirical dispersion-correction with Becke-Johnson damping for B3LYP.² Frequency analysis is used to determine that each reported minimum energy structure has zero imaginary frequencies and each transition state (TS) structure has only one imaginary frequency. Intrinsic reaction coordinate (IRC) calculations were performed for selected transition state structures to correctly identify the reactants and products. Bulk solvent effects are incorporated for geometry optimizations using the self-consistent reaction field polarizable continuum model (IEF-PCM)³⁻⁵ with dichloromethane as the solvent. Thermal corrections for the free energy (G) and enthalpy (H) are calculated at the B3LYP-D3/BS1 level of theory and the free energies are further corrected to a solution standard state of 1M at 298.15 K.⁶⁻⁷ For most cases, the electronic energy of the B3LYP-D3BJ/BS1 optimized geometry is recalculated at the B3LYP-D3BJ/[6-311+G(2d,p) + SDD (Pd, I)] level of theory (B3LYP-D3BJ/BS2) with the PCM model for either methanol or dichloromethane depending on the experimental reaction conditions. Then the thermal corrections (calculated at the B3LYP-D3/BS1 level) are applied to give the final free energy and enthalpy values reported in the text. NBO charges are calculated using the NBO program (version 3.1), as implemented in G09.⁸

S2.2. Comparison of Experimental and Computational Dimer Structures

To gauge how well the computations are able to reproduce the experimental dimeric structures, we make a detailed comparison between the structure determined by x-ray crystallography of the NHAc-Gly carboxylate bridged Pd dimer structure **2** and the corresponding DFT-optimized structure, as shown in Table S2.1. The unit cell for the crystal structure has two molecules of **2**, so the experimental distances are taken as an average. The DFT methodology reproduces the experimentally determined structure with excellent accuracy including the interactions between dmbs fragments observed in NMR experiments.

Table S2.1. Side-by-side comparison of geometric parameters (distances in Å) for the experimentally determined x-ray crystal structure and DFT-optimized structure of the NHAc-Gly Pd dimer structure, **2**.

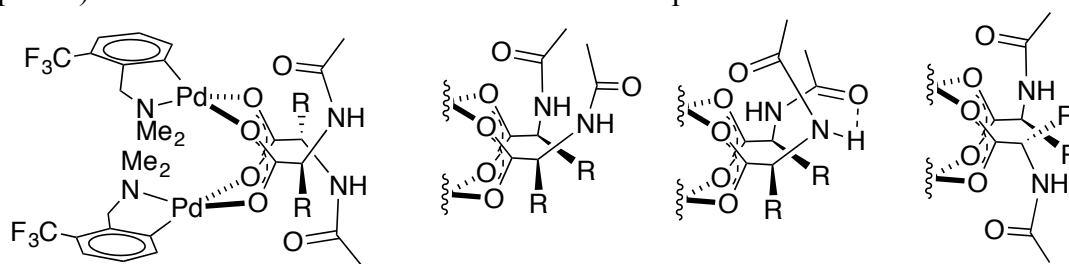


Geometric Parameter	X-ray structure	DFT-optimized structure	Geometric Parameter	X-ray structure	DFT-optimized structure
Pd ¹ -O ¹	2.147	2.206	Pd ¹ -Pd ²	2.962	2.985
Pd ¹ -O ³	2.059	2.100	N ¹ -C ³	4.096	4.037
Pd ¹ -N ¹	2.061	2.122	N ² -C ¹	4.084	4.031
Pd ¹ -C ¹	1.971	1.972	C ² -C ⁴	4.169	3.920
Pd ² -O ²	2.062	2.104	H ¹ -Me ³	3.547	3.607
Pd ² -O ⁴	2.148	2.203	H ² -Me ²	3.587	3.592
Pd ² -N ²	2.058	2.123	O ⁵ -Me ²	3.360	3.363
Pd ² -C ³	1.959	1.972	O ⁶ -Me ³	3.545	3.342

S2.3. Dimerization Energies and Conformations of Dimeric Structures

Several conformations of the MPAA-bridged dimer structures were examined in accord with the determined x-ray crystal structures. Table S2.2 shows the conformations examined (1-4) and their relative energies for four MPAA structures: **6a** (NHAc-Gly), **6b** (NHAc-Ala), **6c** (NHAc-Leu), and **6d** (NHAc-Ile). Remarkably, the crystallographically observed conformation (marked with an * in Table S2) for **6a-c** are also the lowest computed structures. However, especially for NHAc-Gly, the conformations are relatively close in energy indicating some flexibility of the MPAA side chains. Notably, the examined conformation with intramolecular hydrogen bonding (3) is calculated to be one of the higher energy structures in all cases.

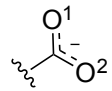
Table S2.2. Dimerization energies (kcal/mol, calculated relative to corresponding monomer complexes) for several conformations of the MPAA complexes **6a-d**.



Conformation	1	2	3	4	
Structure	ΔG_{dimer}	ΔH_{dimer}	Structure	ΔG_{dimer}	ΔH_{dimer}
R = H (Gly)			R = <i>i</i> -Bu (Leu)		
6a-1* (6a)	-18.5	-35.9	6c-1	-13.5	-32.2
6a-2	-18.3	-36.0	6c-2	-17.7	-36.5
6a-3	-17.0	-36.6	6c-3	-16.8	-36.9
6a-4	-17.6	-36.2	6c-4* (6c)	-21.0	-39.0
R = Me (Ala)			R = <i>s</i> -Bu (Ile)		
6b-1	-10.2	-31.3	6d-1	-10.6	-30.1
6b-2* (6b)	-18.5	-36.7	6d-2	-21.5	-39.6
6b-3	-11.4	-33.3	6d-3	-19.4	-39.6
6b-4	-16.8	-37.1	6d-4	-19.4	-37.9

In our previous study on carboxylate-bridged Pd-acetate dimer complexes, we predicted that the presence of electron-withdrawing groups on the carboxylate ligands stabilizes the dimer relative to separated monomers by increasing interaction energy between the Pd-center and ligands (*i.e.* via the Pd-OCO bonding motif).⁹ One way we measured this effect was by calculating the NBO charge on the free (anionic) carboxylate ligands and comparing it to the calculated dimerization energy. We perform the same analysis for MPAA, acetate, and TFA ligands in Table S2.3. In all cases except Ile, the average NBO charge on the carboxylate oxygen atoms of the free ligand (O¹ and O²) correlates well with the calculated dimerization energy suggesting that this electronic effect is at least partially responsible for the observed preference for MPAA-bridged dimers over acetate-bridged dimers. Intriguingly, the electronic effect do not account for the increased stability of the dimer with Ile suggesting that some effects from the increased size of the side chain (e.g., dispersive interactions) may provide additional stabilization.

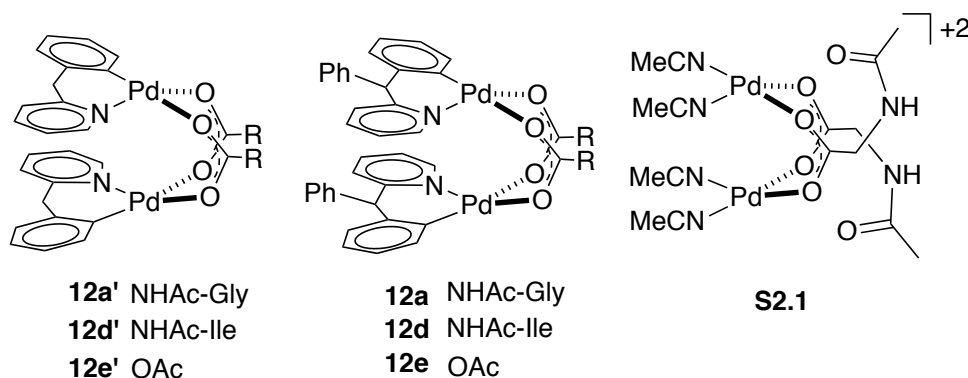
Table S2.3. Side-by-side comparison of dimerization energies (kcal/mol, calculated relative to corresponding monomer complexes) and NBO charges (e) for several bridging carboxylate ligands.

Ligand	$\Delta G_{\text{dimer}}/\Delta H_{\text{dimer}}$	Average NBO charge of carboxylate oxygen atoms for free ligand	NBO charge on O^1/O^2 
Gly	-18.5/-35.9	-0.823	-0.830/-0.815
Ala	-18.5/-36.7	-0.822	-0.830/-0.814
Ile	-21.5/-39.6	-0.821	-0.834/-0.807
Acetate	-17.3/-33.1	-0.844	-0.847/-0.840
TFA (CF ₃ CO ₂)	-20.0/-36.8	-0.773	-0.778/-0.767

S2.4. Substrate Effect

We have also calculated the $\Delta G_{\text{dimer}}/\Delta H_{\text{dimer}}$ values for cyclopalladated carboxylate bridged Pd/MPAA and acetate species with 2-pyridyl-diphenylmethane (**12'a/d/e**) and 2-benzylpyridine (**12a/d/e**) substrates, as well as with acetonitrile (**S2.1**). In all cases, we find that the dimer is favored over the separated two monomers. (These energies are reported at the B3LYP-D3BJ/BS1 level of theory. We do not expect higher level of theory will change the general conclusions gathered here.) As in our previous study, these calculations show that the nature of substrate can have a large impact on the thermodynamic stability of dimeric complexes. Regardless of carboxylate ligand, the additional phenyl substituent of 2-(diphenylmethyl)pyridine stabilizes the corresponding cyclopalladated dimer complex relative to that derived from 2-benzylpyridine. The presented calculations are consistent with the experimental data showing that MPAA-bridged dimeric complexes can form with a wide range of substrates relevant for C-H functionalization.

Table S2.4. Dimerization energies (kcal/mol, calculated relative to corresponding monomer complexes) for several substrates relevant for C-H functionalization and carboxylate ligands.



Structure	ΔG_{dimer}	ΔH_{dimer}
12a'	-37.5	-52.8
12d'	28.8	-50.5
12e'	-28.3	-41.5
12a'	-40.6	-53.1
12d'	-43.7	-56.1
12e'	-31.2	-46.2
S2.1	-24.7	-46.3

S2.5. C-H Activation with MPAA Dimer and Monomer

For the mechanism of cyclopalladation of the dimer, we investigated two mechanisms shown in Figure S2.1: “external acetate”-type (green) and “internal acetate”-type. The “external acetate” mechanism has a calculated free energy barrier of $\Delta G^\ddagger = 29.1$ kcal/mol is higher than the “internal acetate” mechanism, which has a free energy barrier of $\Delta G^\ddagger = 23.2$ kcal/mol. The key difference between these pathways is the dissociating ligand prior to the C-H activation transition state: In the “external acetate”-type mechanism acetate dissociates and in the “internal acetate”-type mechanism one of the bridging carboxylates partially dissociates. However, the reactant (**18-D**), intermediate (**21-D**) and product (**24-D**) complexes are the same for both pathways.

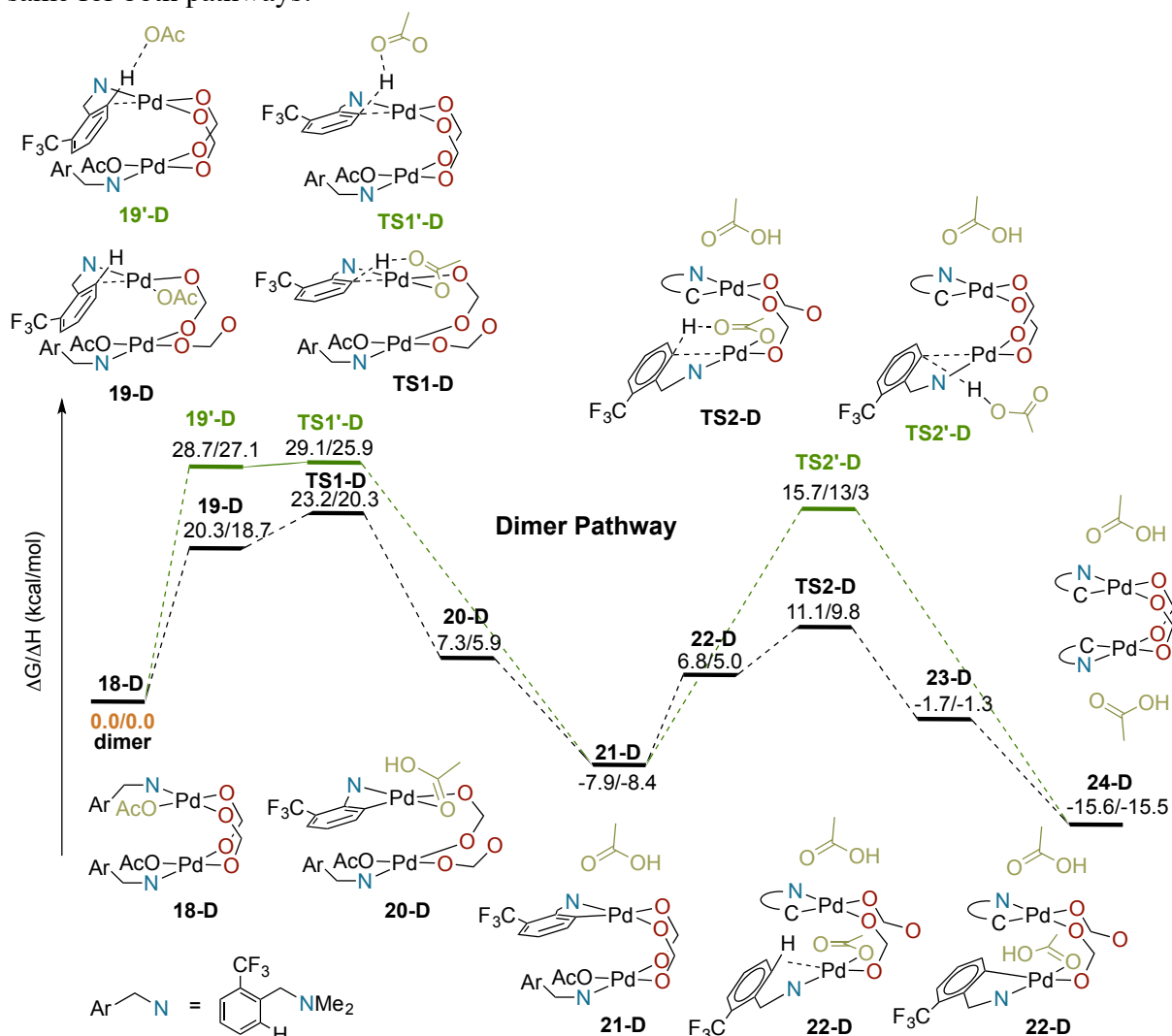


Figure S2.1 Full calculated free energy surface for the double cyclopalladation starting from $[\text{Pd}(\text{II})(\kappa\text{-}N\text{-F}_3\text{C-dmba})(\kappa\text{-OAc})(\mu\text{-NAc-Gly})_2]$ (**18-D**). An “external acetate”-type mechanism (green) and an “internal acetate”-type mechanism (black) were studied.

For the mechanism of cyclopalladation of the monomer, we investigated three mechanisms shown in Figure S2.2: “internal acetate” (black), “internal MPAA” (green), and “external acetate” (blue). The lowest energy pathway is the “internal acetate” pathway with an overall free energy barrier of $\Delta G^\ddagger = 41.7$ kcal/mol. The other pathways have significantly higher free energy barriers of $\Delta G^\ddagger = 47.2$ and 46.0 kcal/mol for the “internal MPAA” and “external acetate” pathways, respectively. All of the examined monomer pathways are higher in energy than the dimer pathway by at least 18 kcal/mol indicating that the dimer pathway is favored.

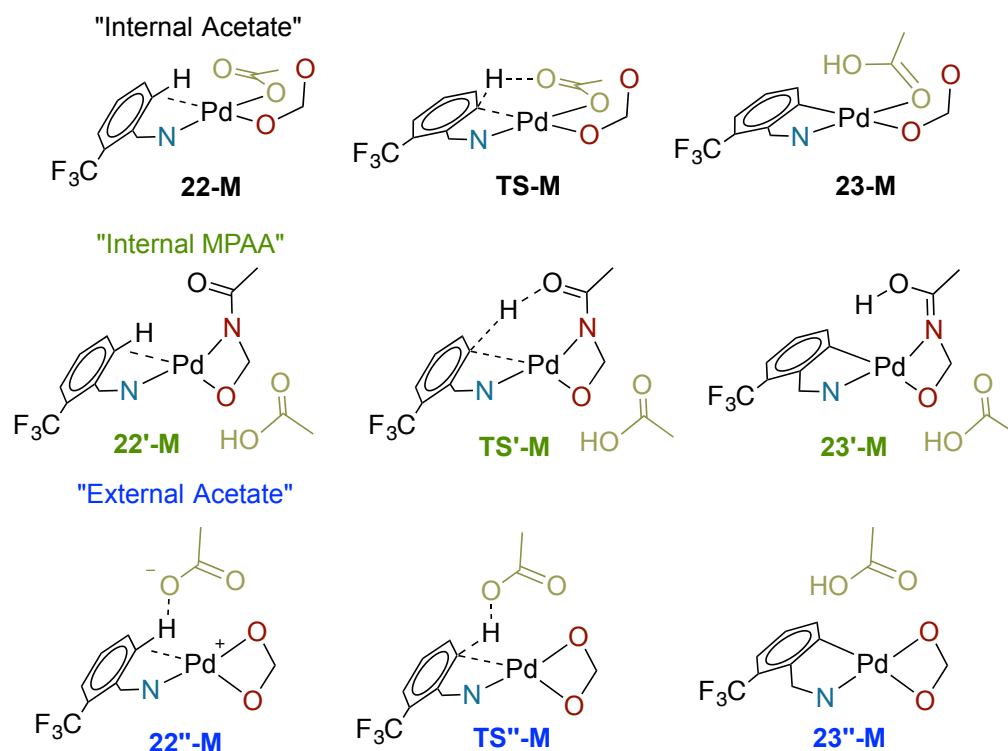
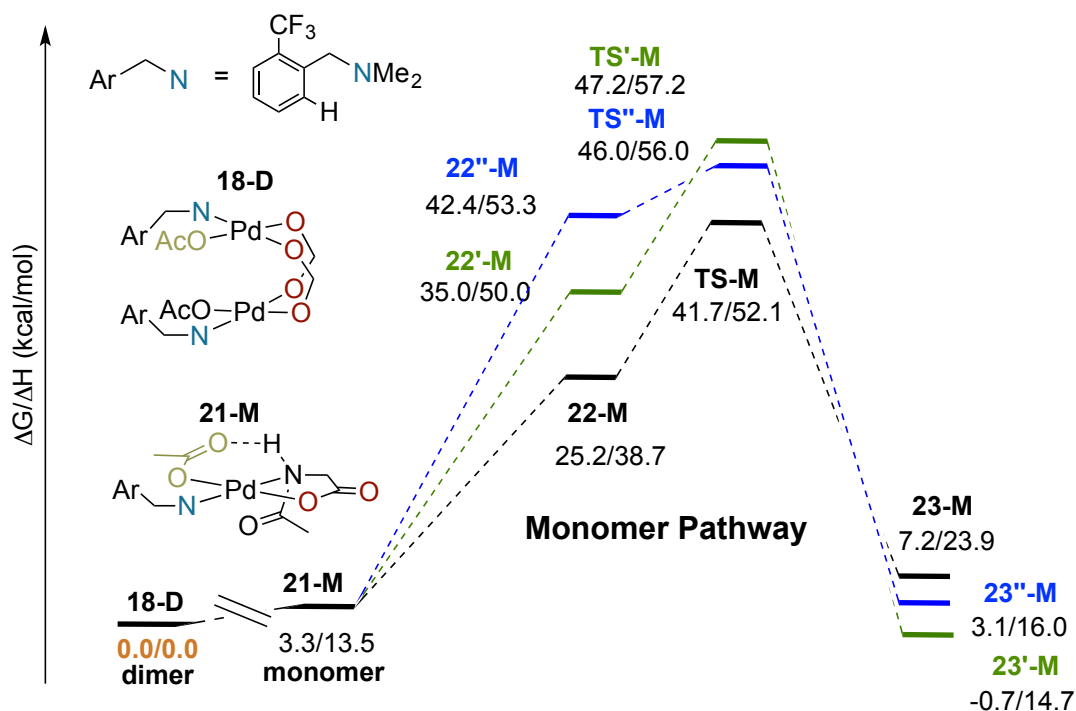


Figure S2.2 Full calculated free energy surface for the double cyclopalladation starting from (F₃C-dmba)Pd(II)/MPAA monomer complex **21-M**. Three pathways were examined: "internal acetate" (black), "internal MPAA" (green), and "external acetate" (blue).

S2.6. Computational Analysis of Pd-C Bond Iodination in Cyclopalladated MPAA Dimer and Monomer Complexes

We previously reported that C-H iodination catalyzed by Pd(II) systems proceeds via a redox-neutral electrophilic cleavage (EC) mechanism as opposed to a Pd(II)/Pd(IV) oxidative addition and reductive elimination sequence.¹⁰ As illustrated in Figure S2.3a, the EC pathway is initiated by coordination of I₂ to the Pd(II) center as a Z-type ligand.¹¹ In the transition state, C-I bond formation and I-I bond cleavage occur in a concerted fashion without formal oxidation of the Pd(II). We also examined the effect of the nuclearity of the reactive Pd(II) species on the EC barrier and found that the reaction is faster with the acetate-bridged dimer than with the corresponding monomer.¹⁰ The experimental observation of participation of exogenous iodide on the reaction with I₂ led us to investigate the effect of iodide on the reaction of **6a** with I₂ through the EC pathway. We hypothesized that coordination of iodide *trans* to the reactive, Z-type I₂ would activate the I-I bond and create a more nucleophilic palladate leading to acceleration of the electrophilic iodination process.^{12,13}

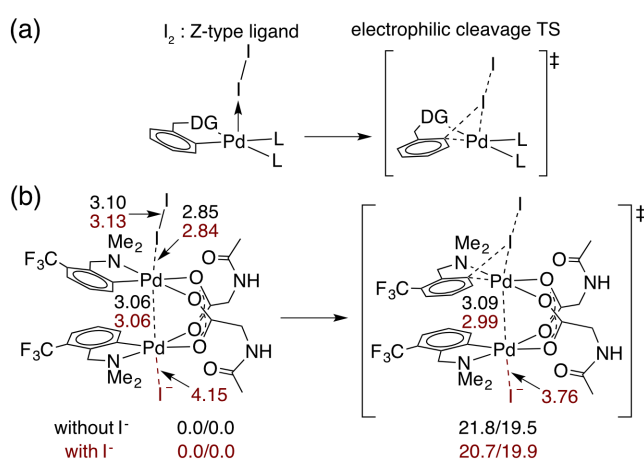


Figure S2.3 (a) General reaction pathway for the redox-neutral electrophilic cleavage (EC) mechanism for C-I bond formation; (b) Results from DFT calculations showing how iodide generated during the reaction accelerates EC with **2a** and I₂

Indeed, the free energy barriers ($\Delta G_{\text{EC}}^{\ddagger}$) for iodination through the EC pathway with and without iodide coordination to the second Pd-center are calculated to be 20.7 and 21.8 kcal/mol, respectively. The calculated decrease in $\Delta G_{\text{EC}}^{\ddagger}$ by 1.0 kcal/mol suggests a role for exogenous iodide in the iodination reaction consistent with our hypothesis. Careful examination of the geometric features of the reactants and transition states show in Figures S2.3 b and S2.4 provides some insight into how iodide accelerates the EC pathway: 1) The I-I bond is slightly elongated in the presence of iodide (3.13 and 3.10 Å with and without iodide, respectively) indicating that I₂ is more activated¹⁰, and 2) In the transition state, the Pd-Pd distance decreases in the presence of iodide (2.99 and 3.09 Å with and without iodide, respectively) indicating that the iodide facilitates participation¹⁴⁻¹⁶ of the second Pd center in the transition state. Therefore, based on these computational results the generation of iodide during the reaction accelerates iodination and may do so by the formation of more nucleophilic iodo-palladate.

S2.7. Energies for Calculated Structures

The electronic energies (in hartrees) calculated at B3LYP-D3BJ/BS1 and B3LYP-D3BJ/BS2 levels of theory are provided, as well as the applied zero point energy (ZPE), enthalpy (H) and corrected (solution state of 1M) Gibbs free energy (G°) corrections calculated at the B3LYP-D3/BS1 level for all structures. Energies calculated with the PCM model for methanol are noted (MeOH) and all other energies are calculated in dichloromethane. Imaginary frequencies are provided for transition structures. Throughout this document **-D** and **-M** indicate calculated dimeric and monomeric species, respectively

Table S2.5. Computed energies (hartree) for dimerization and ligand exchange

Structure	E(BS1)	E(BS2) (MeOH)	ZPE	H	G°	Im. Freq.
1	-968.311629	-969.752565	0.301753	0.322415	0.255567	none
2	-1936.700074	-1939.559493	0.605550	0.647731	0.531102	none
2-μ-(N,O)	-1936.679454	-1939.536864	0.606079	0.648098	0.533912	none
3	-968.312282	-969.750682	0.300597	0.322032	0.250500	none
NHAc-Gly-CO₂H	-437.137356	-437.282299	0.117395	0.127341	0.084516	none
NHAc-Gly-CO₂⁻	-436.649703	-436.823022	0.104625	0.114064	0.072956	none
6a-M	-1305.354058	-1306.916199	0.305613	0.330562	0.251763	none
6a-1 (6a)	-2610.789385	-2613.893475	0.615943	0.664957	0.535117	none
6a-2	-2610.789912	-2613.893411	0.615672	0.664756	0.535408	none
6a-3	-2610.793589	-2613.894603	0.616566	0.664996	0.538573	none
6a-4	-2610.791091	-2613.893882	0.616027	0.664952	0.536988	none
NHAc-Ala-CO₂H	-476.462760	-476.614900	0.145788	0.156981	0.112152	none
NHAc-Ala-CO₂⁻	-475.974820	-476.154240	0.132627	0.143472	0.099366	none
6b-M	-1344.679036	-1346.248901	0.333509	0.359970	0.276683	none
6b-1	-2689.432996	-2692.552124	0.672784	0.724348	0.591406	none
6b-2	-2689.436985	-2692.559693	0.670928	0.723350	0.585718	none
6b-3	-2689.437723	-2692.554978	0.672710	0.724065	0.592308	none
6b-4	-2689.440310	-2692.560793	0.671911	0.723867	0.589539	none
6c-M	-1462.643914	-1464.240661	0.419367	0.449633	0.358415	none
6c-1	-2925.361906	-2928.536157	0.843020	0.902854	0.750122	none
6c-2	-2925.368319	-2928.542906	0.842640	0.902643	0.750260	none
6c-3	-2925.368811	-2928.541158	0.843327	0.902844	0.753140	none
6c-4 (6c)	-2925.370855	-2928.546683	0.842463	0.902518	0.748721	none
NHAc-Ile-CO₂H	-594.427709	-594.604270	0.231602	0.246704	0.192713	none
NHAc-Ile-CO₂⁻	-593.938035	-594.140625	0.218642	0.233221	0.180878	none
6d-M	-1462.642921	-1464.238797	0.419583	0.449877	0.358332	none
6d-1	-2925.356665	-2928.529025	0.843330	0.903141	0.751231	none
6d-2	-2925.367902	-2928.543609	0.842357	0.902692	0.748454	none
6d-3	-2925.370403	-2928.543972	0.842357	0.902692	0.748454	none
6d-4	-2925.365220	-2928.541614	0.843321	0.903361	0.749715	none
AcOH	-229.104141	-229.184238	0.061825	0.067331	0.037681	none
AcO⁻	-228.601288	-228.715083	0.048588	0.053895	0.024482	none
9-M	-1097.311775	-1098.815602	0.250769	0.270932	0.204556	none
9	-2194.703505	-2197.686747	0.504464	0.544643	0.437165	none
10	-2402.753525	-2405.790216	0.559848	0.604508	0.485793	none
CF₃CO₂H	-526.801635	-526.993792	0.038931	0.046154	0.010136	none
CF₃CO₂⁻	-526.327658	-526.551340	0.026040	0.032991	-0.001907	none
9-TFA-M	-1395.025373	-1396.633986	0.227115	0.249435	0.176784	none
9-TFA	-2790.130485	-2793.329728	0.457849	0.502042	0.383387	none

Table S2.6. Computed energies (hartree) for dimerization of C-H functionalization relevant substrates

Structure	E(BS1)	E(BS2) (MeOH)	ZPE	H	G°	Im. Freq.
12a'-M	-1081.444973	-	0.295935	0.316994	0.247690	none
12a'-D	-2162.979018	-	0.596446	0.638929	0.521640	none
12d'-M	-1238.734027	-	0.409899	0.437232	0.349869	none
12d'-D	-2477.552946	-	0.825422	0.878846	0.738733	none
12e'-M	-873.417426	-	0.240552	0.257994	0.196986	none
12e'-D	-1746.903757	-	0.483719	0.518761	0.417828	none
12a-M	-1312.527964	-	0.376950	0.402708	0.322535	none
12a-D	-2625.146580	-	0.758561	0.811434	0.671059	none
12d-M	-1469.817049	-	0.490693	0.520965	0.431711	none
12d-D	-2939.732452	-	0.988495	1.050851	0.892207	none
12e-M	-1104.493368	-	0.321678	0.343765	0.270873	none
12e-D	-2209.063395	-	0.646221	0.690559	0.568671	none
S2.1-M	-828.688663	-	0.202043	0.222722	0.151629	none
S2.1-D	-1657.454797	-	0.409987	0.449185	0.341407	none

Table S2.7. Computed energies (hartree) for MPAA dimer and monomer cyclopalladation pathways

Structure	E(BS1)	E(BS2) (MeOH)	ZPE	H	G°	Im. Freq.
18-D	-3069.009008	-3072.265561	0.745378	0.805698	0.646984	none
19-D	-3068.977734	-3072.234624	0.744264	0.804633	0.648325	none
TS1-D	-3068.967134	-3072.226614	0.739414	0.799137	0.645029	1059.3i
20-D	-3068.995310	-3072.255655	0.744806	0.805152	0.648713	none
21-D	-3069.022305	-3072.277872	0.743810	0.804559	0.646735	none
22-D	-3069.002805	-3072.256316	0.744097	0.804481	0.648509	none
TS2-D	-3068.984931	-3072.242388	0.738025	0.798204	0.641513	1253.3i
23-D	-3069.012127	-3072.266094	0.743094	0.804089	0.644804	none
24-D	-3069.034389	-3072.288110	0.742543	0.803604	0.644603	none
19'-D	-3068.962811	-3072.219728	0.742665	0.803094	0.646836	none
TS1'-D	-3068.962792	-3072.219800	0.741622	0.801233	0.647598	21.6i
TS2'-D	-3068.984275	-3072.237952	0.739343	0.799312	0.644362	178.8i
21-M	-1534.485355	-1536.120207	0.371631	0.400999	0.313559	none
22-M	-1534.462129	-1536.099146	0.369512	0.400045	0.309908	none
TS-M	-1534.444487	-1536.081794	0.364249	0.393396	0.305740	1215.0i
23-M	-1534.471885	-1536.111158	0.369646	0.400307	0.307580	none
22'-M	-1534.452426	-1536.089175	0.368889	0.399093	0.307769	none
TS'-M	-1534.441280	-1536.077995	0.364184	0.393666	0.306348	1093.3i
23'-M	-1534.479470	-1536.117933	0.369650	0.399706	0.308075	none
22''-M	-1534.451322	-1536.086348	0.369217	0.398913	0.310848	none
TS''-M	-1534.442143	-1536.079518	0.364878	0.394186	0.306843	719.0i
23''-M	-1534.477583	-1536.117739	0.370435	0.400584	0.310942	none

Table S2.8. Computed energies (hartree) for iodination

Structure	E(BS1)	E(BS2)	ZPE	H	G°	Im. Freq.
26	-2633.593117	-2636.761782	0.617436	0.671332	0.526090	none
26-TSI	-2633.567834	-2636.730077	0.617773	0.670734	0.529099	49.6i
27	-2645.165340	-2648.371707	0.618413	0.674369	0.523126	none
27-TSI	-2645.138514	-2648.339002	0.617965	0.673309	0.523481	41.8i

S2.8. References

1. Gaussian 09, Revision E.01, Frisch, M. J.; Trucks, G. W.; Schlegel, H. B.; Scuseria, G. E.; Robb, M. A.; Cheeseman, J. R.; Scalmani, G.; Barone, V.; Mennucci, B.; Petersson, G. A.; Nakatsuji, H.; Caricato, M.; Li, X.; Hratchian, H. P.; Izmaylov, A. F.; Bloino, J.; Zheng, G.; Sonnenberg, J. L.; Hada, M.; Ehara, M.; Toyota, K.; Fukuda, R.; Hasegawa, J.; Ishida, M.; Nakajima, T.; Honda, Y.; Kitao, O.; Nakai, H.; Vreven, T.; Montgomery, J. A., Jr.; Peralta, J. E.; Ogliaro, F.; Bearpark, M.; Heyd, J. J.; Brothers, E.; Kudin, K. N.; Staroverov, V. N.; Kobayashi, R.; Normand, J.; Raghavachari, K.; Rendell, A.; Burant, J. C.; Iyengar, S. S.; Tomasi, J.; Cossi, M.; Rega, N.; Millam, M. J.; Klene, M.; Knox, J. E.; Cross, J. B.; Bakken, V.; Adamo, C.; Jaramillo, J.; Gomperts, R.; Stratmann, R. E.; Yazyev, O.; Austin, A. J.; Cammi, R.; Pomelli, C.; Ochterski, J. W.; Martin, R. L.; Morokuma, K.; Zakrzewski, V. G.; Voth, G. A.; Salvador, P.; Dannenberg, J. J.; Dapprich, S.; Daniels, A. D.; Farkas, Ö.; Foresman, J. B.; Ortiz, J. V.; Cioslowski, J.; Fox, D. J. Gaussian, Inc., Wallingford CT, 2009.
2. Grimme, S.; Antony, J.; Ehrlich, S.; Krieg, H. *J. Chem. Phys.* **2010**, *132*, 154104-154119.
3. Cancès, E.; Mennucci, B.; Tomasi, J. *J. Chem. Phys.* **1997**, *107*, 3032-3041.
4. Mennucci, B.; Tomasi, J. *J. Chem. Phys.* **1997**, *106*, 5151-5158.
5. Scalmani, G.; Frisch, M. J. *J. Chem. Phys.* **2010**, *132*, 114110-114124.
6. Essafi, S.; Tomasi, S.; Aggarwal, V. K.; Harvey, J. N. *J. Org. Chem.* **2014**, *79*, 12148-12158.
7. Plata, R. E.; Singleton, D. A. *J. Am. Chem. Soc.* **2015**, *137*, 3811-3826.
8. Glendening, E. D.; Reed, A. E.; Carpenter, J. E.; Weinhold, F. NBO, version 3.1; University of Wisconsin: Madison, WI, 1996.
9. Haines, B. E.; Berry, J. F.; Yu, J. Q.; Musaev, D. G. *ACS Catal.* **2016**, *6*, 829-839.
10. Haines, B. E.; Xu, H.; Verma, P.; Wang, X.-C.; Yu, J.-Q.; Musaev, D. G. *J. Am. Chem. Soc.* **2015**, *137* (28), 9022.
11. Rogachev, A. Y.; Hoffmann, R. *J. Am. Chem. Soc.* **2013**, *135*, 3262.
12. Powers, D. C.; Xiao, D. Y.; Geibel, M. A. L.; Ritter, T. *J. Am. Chem. Soc.* **2010**, *132*, 14530.
13. Umakoshi, K.; Ichimura, A.; Kinoshita, I.; Ooi, S. *Inorg. Chem.* **1990**, *29*, 4005.
14. Powers, D. C.; Ritter, T. *Acc. Chem. Res.* **2012**, *45*, 840.
15. Powers, D. C.; Ritter, T. *Organometallics* **2013**, *32*, 2042.
16. Kornecki, K. P.; Berry, J. F.; Powers, D. C.; Ritter, T. In *Progress in Inorganic Chemistry Volume 58*; Progress in Inorganic Chemistry; John Wiley & Sons, Inc.: Hoboken, New Jersey, 2014; pp 225–302.